# CHAPTER 4
# THE LIDAR RECEIVER

Two different kinds of lidar receiver have been designed. The first one is an analogically controlled receiver while the second one is digitally controlled.

The chapter begins with a review of different photodiode sensing circuits wherefrom the transimpedance circuit is justified. The design is based on the receiver specifications given in Chap.3 and on the analog configuration. Careful choice of operational amplifiers (op amps) and the incorporation of new technologies available such as CFA have made ends met. Appendix 1 discusses CFAs in more detail.

Other sections of the chapter concentrate on the layout, electronics, mechanics and test and measurement of the analog prototype. Particular attention is devoted to thermal drift of the optoelectronic receiver and its role on the actual lidar application.

## 1. SPECIFICATIONS OVERVIEW

*Lidar receiver specs from Tab.3. Chap.3. are reproduced below:*

Estimated system absolute ranges and typical power levels

$R_{min}{}^{a} < 200$ m ($P \approx 5$ mW) $\qquad R_{max}{}^{a} \geq 5$ km ($P \approx 5$ nW)

Assuming: $L=0.3$, $R_{io}$(specs) $= 0.3$ A/W, M(specs) $\epsilon$ (1,120), $V_{sat}= 1$V

Chain gain, M·G ($G=G_T \cdot G_A$):

$$MG \leq 4400\ \Omega;\ MG \geq 8.7 \cdot 10^6\ \Omega$$

if M $\epsilon$ (1,120) then

$$\mathbf{G_{min} \leq 4400\ \Omega;\ G_{max} \geq 72 \cdot 10^3\ \Omega}$$

Bandwidth (sampling rate 20 MHz): **B < 10 MHz**

Further specs: Variable gain between $G_{min}$, $G_{max}$ and offset (-1 V level shift).

***Tab.1 Receiver specs summary (Tab.3, Chap.3)***

## 2. SENSING CIRCUITS FOR THE LIDAR FRONT-END

### 2.1 I-V characteristics

With no illumination on the photodiode, the *I-V* characteristic is similar to that of a rectifying diode curve. The dark current expression

$$I_d = I_s \left[ \exp\left( \frac{qV}{KT} \right) - 1 \right] \qquad (1)$$

where

$I_d$ is the dark current,

$I_s$ is the reverse saturation current,

$q$ is the electron charge,

$V$ is the applied bias voltage,

$K$ is the Boltzmann's constant and,

$T$ is the absolute temperature,

shows the relationship of the dark current as a function of applied bias and temperature. Illuminating the photodiode with optical radiation shifts the *I-V* curve by the amount of photocurrent generated, $I_p$

$$I_p = R_i P_s \tag{2}$$

where

$R_i$ is the current responsivity and,

$P_s$ is the illuminating optical power.

By merging eqs.(1) and (2), the total current in the presence of light becomes

$$I = I_s\left[\exp\left(\frac{qV}{KT}\right) - 1\right] - I_p \tag{3}$$

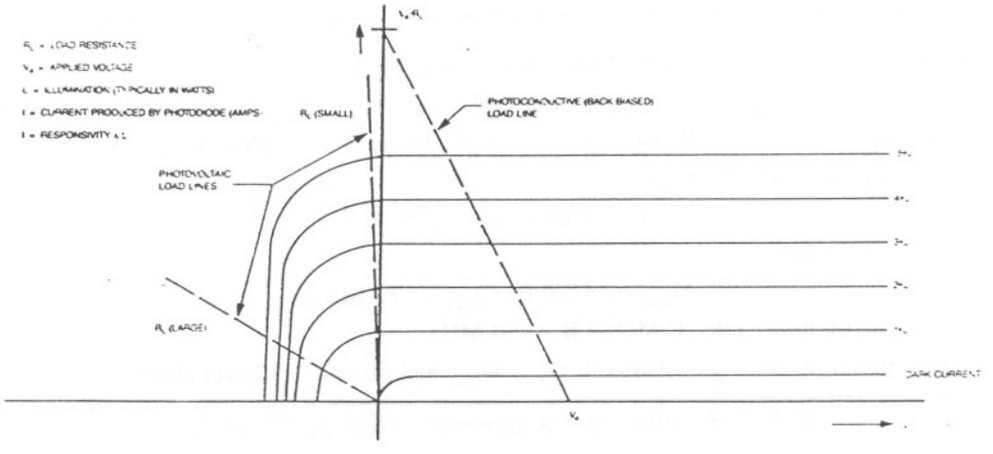


***Fig.1 Photodiode I_V characteristics with load line [107].***

The external circuit to which a photodiode is connected usually contains a current-to-voltage element such as a resistor (passive) or a transimpedance operational amplifier (active). In addition, the photodiode may be operated in the *photovoltaic (PV) unbiased mode, or in the photoconductive (PC) mode, where a reverse bias is applied.*

Fig.1 shows the characteristic photodiode I-V curves. A load line for the photoconductive (reverse bias) modes is shown on the section of the graph to the right of the zero voltage line, and a load line for the photovoltaic mode is shown to the left of the zero voltage line. *V-axis* is negative to the right and *I-axis* is negative upwards.

The photodiode operating point is found where the *I-V* characteristic of the load (load line) intersects the photodiode I-V characteristic. In the photovoltaic mode, the load line passes through the origin and intersects the photodiode characteristic near the *knee*.

In the photoconductive mode, the load line is shifted by the bias voltage and *intersects the photodiode characteristic in the flatter portion.* Operating the photodiode with and external reverse bias extends the linearity of the circuit and its bandwidth (better rise time). This is because applying a reverse bias reduces the junction capacitance:

$$C_j = \frac{kA_d}{\sqrt{\rho\,(V_{bi}+V_{br})}} \qquad [pF] \tag{4}$$

where

$C_j$ is the junction capacitance [pF],
$k$ is a manufacturer's constant (19200 for UDT [107]),
$A_d$ is the photodiode active area [cm$^2$],
$V_{bi}$ is the contact potential [V],
$V_{br}$ is the applied reverse bias [V] and,
$\rho$ is the resistivity of the semiconductor in the depleted layer [Ω·cm].

In addition, *the slope of the load line is* $m=1/R_L$, where $R_L$ is the load. The disadvantage of using a reverse bias is an increase in photodiode dark current. Another point is that linearity is ultimately limited by carrier generation (the number of photons impinging on the active area of the photodiode becomes comparable to the number of electron-holes centres) [153]. *Both effects, load and carrier generation must be regarded.* When the diode works as an APD, the back biased polarization (photoconductive mode) is implicit and in addition to increased linearity, it carries a multiplication gain as well.

Providing and effective short circuit to the load of the photodiode prevents a load voltage from being developed, and the photodiode does not become forward-biased, avoiding the inherent clampling action of the diode. A virtual ground obtained by an operational amplifier is often used to minimize the load to the photodiode. The operational acts as a current to voltage converter with the output signal amplified by a large feedback resistor $R_F$

$$V_{o1} = -IR_F \tag{5}$$

where

$V_{o1}$ is the voltage a the output of the transimpedance amplifier
(subscript *1* indicates first amplification stage in the circuit diagram of Fig.2),
$I$ is the photocurrent and,
$R_F$ is the feedback resistor or transimpedance gain.

In such circuit, the effective detector load resistance is

$$R_L = \frac{R_F}{A_o}\ ; \qquad R_{sh} \gg R_F\ ,\quad A_o \gg 1+\frac{R_F}{R_{sh}} \tag{6}$$

where

$A_o$ is the open-loop gain of the op amp and,
$R_{sh}$ is the shunt resistance of the photodiode.

The above considerations led to the design of a configuration with the photodiode operated at reverse bias and followed by a *transimpedance amplifier (TIA) configuration (Fig.2).* In the figure, the photodiode is connected through a jumper to a *high voltage supply (HVS),* which applies the reverse bias to the device. In one position, the jumper connects the APD directly to the HVS, while in the other, a *10-kΩ resistor,* $R_{APD}$, is connected in series. This resistance is installed to limit the maximum current across the photodiode. For instance, unwanted polarity errors in the HVS or extremely high light levels (e.g. at *15 V,* direct current limit is about *1.45 mA*). For the lidar system, a *digitally programmable HVS (Stanford Research Systems, Inc. Mod. PS350 / 5000V-25W)* has been chosen. Maximum ratings such as current limit, current trip and voltage limit can be easily programmed to ensure full protection to the photodiode.

As for bandwidth and time response, the photodiode puts no limitations at all. From Tab.2, APD bandwidth is about *500 MHz,* much larger that the receiver one *(10 MHz).*

**PHOTODETECTOR PARAMETERS SPECS (APD C30954)**
**(cont. Tab.2. Chap.3)**

| | | |
|---|---|---|
| ***Maximum ratings*** | | |
| Reverse bias current: | 200 μA | |
| Forward current: | 5 mA (average value, continuous operation) | |
| Max. Power dissipation at 22°C: | 100 mW (with heat sink cooling to case) | |
| ***Electrical characteristics*** | | |
| Breakdown voltage: | 375 V (typ); 300 V (min), 475 V (max) | |
| Gain, M (typ): | 120 | |
| Responsivity, $R_i$ (typ-min): | 75-65 A/W (900 nm) | 36-30 A/W (1060 nm) |
| Quantum efficiency, η (typ): | 85 % (900 nm) | 36 % (1060 nm) |
| Dark current: | 50 nA (typ); | 100 nA (max) |
| Series resistance, $R_s$ | | 15 Ω (max) |
| Capacitance: | 2 pF (typ) | 3 pF (max) |
| Rise and fall time (10%-90%): | 2 ns (typ) | 3 ns (max) |

*Tab.2 APD specifications.*

## 2.2 Practical transimpedance amplifiers

The maximum performance of a photodiode used with a transimpedance amplifier is usually determined by the amplifier itself. Major limiting parameters to the receiver include ***input bias current, Gain-Bandwidth Product (GBP), input voltage noise and current noise.*** For the lidar application, these factors have been considered to determine the overall sensing circuit performance.

The amplifier bias current is additive to the detector current (which includes dark current). Bipolar amplifiers have typical bias currents that range from *30-100 nA*. Popular BiFET (BJT-JFET compatible technology) products are the *LF355/6/7* series (National Semiconductor), with input bias currents of $I_B = 30\ pA$ and input offset currents of $I_{OS} = 5\ pA$. JFET-input op amps are also available with sub-picoampere current specifications. One case studied during the design steps of the receiver was the *OPA-128* op amp (Burr-Brown), which uses special JFET structures and isolation techniques to achieve bias currents below *100 fA*. Yet, all these categories of amplifiers suffer from poor bandwidths. This is because these devices find application in connection with low-bandwidth instrumentation applications, such as pH-meters and low speed precision light sensors.

A further practical limitation in op amps is the *input offset voltage,* $V_{OS}$. This is to say that to force the op amp output to zero, a suitable correction voltage must be applied to its input. Browsing through linear data books, very low offset voltage ratings are about a few tens of $\mu V$ [135]. Yet, *low offset temperature drift* is of more concern that the offset figure in itself.

In Chap.3, Sect.2.5.1, it was agreed that the lidar receiver should include a variable offset low-drift facility. In Fig.2, a temperature compensated stage provides a well stabilized bias to shift the output level down to *-1 V* (or other desired level). If the receiver output is feedback to this unit, offset thermal drift correction is possible. This option, which can be set by a jumper, is quite valuable when the receiver works as an optical communications receiver. When the receiver works in the lidar application, *dc coupling* is necessary (Chap.3, Sect.2.5.1) and thus, no offset feedback is possible. Since the unit basically works as a level shifter, *thermal drift correction* is no longer possible and as a result, long-term offsets must be periodically reset. As for the digital receiver, thermal drift cancellation is achieved using an adaptive correction. Ref.[132] gives some guidelines to design bandpass composite amplifiers for low offset and drift.

Wide-band, low noise *TIA* design is also necessary. Of these two requirements, bandwidth is the hardest limitation of all. For instance, a classic $\mu A741$ has an open-loop dc gain of $2x10^5$ and a transition frequency, $f_T = 1MHz$. More expensive op amp types such as *LF353* dual BiFET exhibit $f_T = 4\ MHz$, and the best ones may have $f_T > 20\ MHz$ *[135]*. Still, these figures are too low to meet the receiver specs.

***In the case of the lidar receiver, bandwidth specs have been achieved by cascading a high performance classic voltage-feedback amplifier to a current-feedback amplifier (CFA).*** Thus, the design combines amplifiers of less individual gain but wider bandwidth. These two stages are indicated in Fig.2 as *transimpedance stage* and *conditioning stage.*

***The major breakthrough about CFA amplifiers is that they do no longer work under the classic gain-bandwidth trade-off. The ability to control gain independently of bandwidth constitutes the most outstanding advantage of CF amps over conventional op amps (see. Appendix 1).***

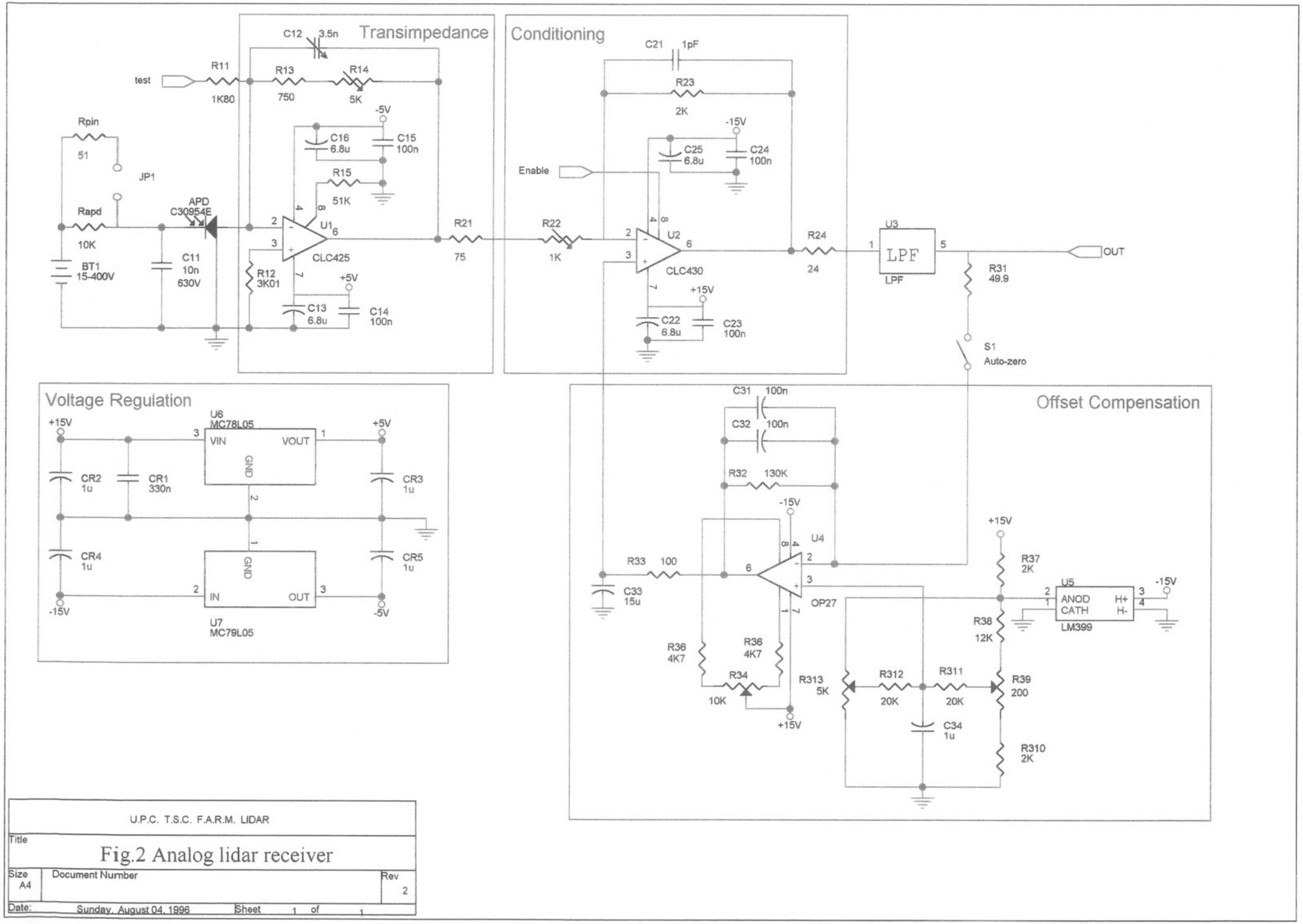


| | | |
|---|---|---|
| U.P.C. T.S.C. F.A.R.M. LIDAR | | |
| Title: Fig.2 Analog lidar receiver | | |
| Size: A4 | Document Number | Rev: 2 |
| Date: Sunday, August 04, 1996 | Sheet 1 of 1 | |

## 3. TRANSIMPEDANCE STAGE

*CLC425* op amp in the transimpedance stage of Fig.2 combines a wide bandwidth ***(1.9GHz)*** with very low input noise ***($1.05nV\cdot Hz^{-1/2}$, $1.6pA\cdot Hz^{-1/2}$)*** and low dc-errors ***(100μV $V_{OS}$, 2μV/°C drift)*** to provide a very precise, wide dynamic-range.

According to Tab.1 receiver specs, *CLC425* op amp is singularly suited for very wide-band high-gain operation. It employs a traditional voltage-feedback topology providing all the benefits of balanced inputs. Going back to Sect.2.2 this means low offsets and drifts, as well as a *96-dB* open-loop gain, *100-dB CMRR* and *95-dB PSRR* (power supply rejection ratio).

Furthermore, *CLC425* offers great flexibility since it includes a provision to externally adjust the supply current. This enables to easily choose the optimum set of power, bandwidth, noise and distortion performance. In the design of Fig.2, the supply current adjustment is done via the resistor $R_{15}$. Taking up manufacturer's advice, this resistor is set to $R_{15}$= *50 kΩ*, thus providing minimum noise, and maximum electrical performance at the expense of a higher consumption ($I_{cc}$=*17 mA)*. In particular, Fig.3 and Fig.4 evidence higher open-loop gains and lower equivalent input noise as long the supply current increases.

In addition to looking for excellent *CMRR* (common mode rejection ratio), from the beginning, a design goal was to look for op amps with very good *PSRR* (power supply rejection ratio). This is so, because the lidar receiver is to be mounted onto the telescope's ocular mount, and the whole set housed into a dome. In order to cope with interference spikes and power supply ripple reaching the equipment in the dome, this parameter is of prime concern. Fig.5 depicts CMRR and PSRR (dB) versus frequency.

On the other hand, *CLC425* main drawback is the reduced output voltage swing. Fig.6 illustrates maximum output swing vs. frequency, under *1-kΩ* load. Up to the maximum frequency of interest *(10 MHz)* output swing is about ±*3.8 V*. When loaded with *50-Ω* output swing falls to ±*3.0 V*. That is why, in Chap.3, Sect.2.5.1 *the input range of the digitizer was chosen to be ±1 V.*

Before proceeding further it is worth noting that the transimpedance stage of Fig.2 includes clamping diodes to protect both common and differential mode voltage ratings [131]. Except for some tests as inverting amplifier, this protection has been removed.

Regarding Sect.2.2, noise is a concerning factor at the transimpedance stage. Fig.7 describes the noise model for the non-inverting amplifier configuration showing all noise sources. (Since transimpedance, inverting and non-inverting configurations with grounded input terminals coincide, this topology will be used as a general configuration). In addition to the intrinsic input voltage noise, $e_n$, and current noise ($i_{n+}$, $i_{n-}$) sources, there also exists thermal voltage noise

$$e_t = \sqrt{4KTR} \tag{7}$$

associated with each of the external resistors. In the figure, $R_{s,eq}$ is the equivalent source

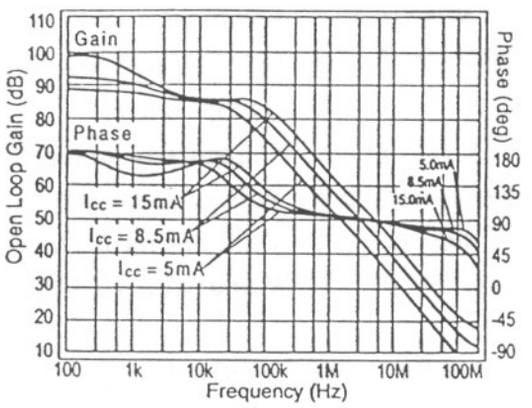


*Fig.3 Open-loop gain and phase vs. $I_{cc}$.*

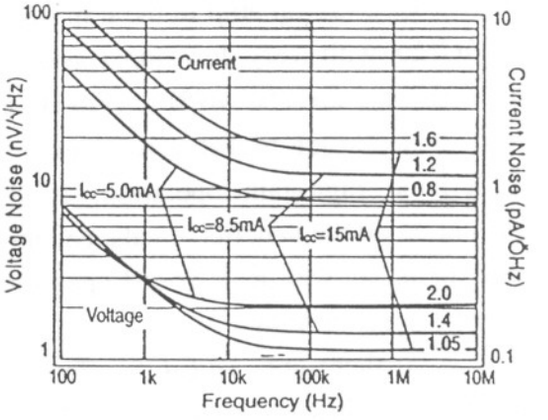


*Fig.4 Equivalent input noise.*

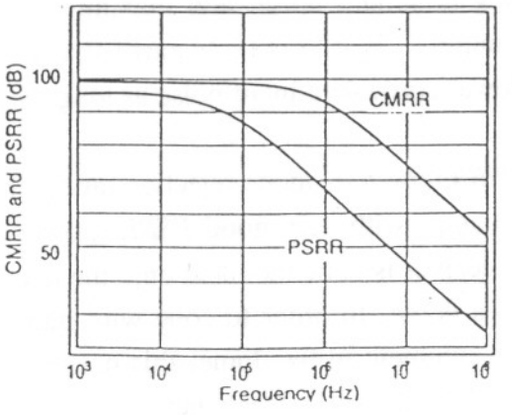


*Fig.5 CMRR and PSRR.*

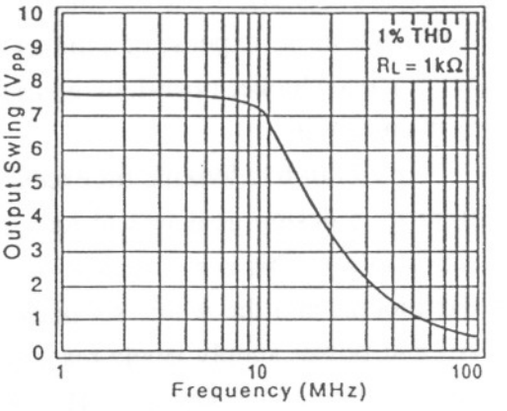


*Fig.6 Maximum output swing.*

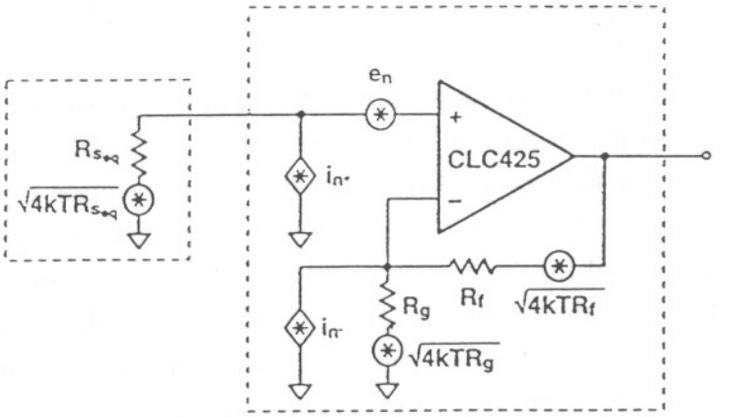


*Fig.7 Non-inverting amplifier noise model.*

*NOTE: Illustrations show CLC425 typical performance from manufacturer's data sheets.*

resistance. Total equivalent input voltage noise density ($e_{ni}$) can be written as:

$$e_{ni} = \sqrt{e_n^2 + (i_{n+}R_{s,eq})^2 + 4KTR_{s,eq} + (i_{n-}(R_f \parallel R_g))^2 + 4KT(R_f \parallel R_g)} \tag{8}$$

If $R_g \to \infty$, $Rb \to 0$ in Fig.7, the transimpedance configuration of Fig.8 comes about. Then, eq.(8) becomes

$$i_{ni} = \sqrt{i_{n-}^2 + \left(\frac{e_n}{R_f}\right)^2 + \frac{4KT}{R_f} + \left(i_{n+}^2 + \frac{4KTR_b}{R_f^2}\right)} \tag{9}$$

Bias current cancellation is accomplished for the transimpedance configuration by placing a resistor, $R_b$, on the non-inverting input equal in value to the feedback resistor (or transimpedance gain), $R_f$. Since the lidar receiver includes an offset correction stage, the final design of Fig.2 does not incorporate $R_b$ in order to avoid the additional noise contribution of the resistor. Then, taking $R_b = 0$ and assuming $i_n = i_{n+} = i_{n-}$, eq.(9) yields

$$i_{ni} = \sqrt{i_n^2 + \left(\frac{e_n}{R_f}\right)^2 + \frac{4KT}{R_f}} \tag{10}$$

Fig.9 plots the basic transimpedance configuration outlined against feedback resistance, $R_f$. The total equivalent output voltage noise density, $e_{no}$ is $i_{ni}R_f$.

Tab.3 summarizes feedback resistor values along with their equivalent input current noise for the final design of Fig.2. Feedback resistor $R_f$ or equivalently, first stage gain, has been made as large as possible during test and characterization of the amplifier. Parasitic capacitances on the inverting and output pins are very critical and very often cause peaking in the frequency response or even circuit oscillation [125][137]. High frequency layout and power supply decoupling with ferrite coils are used.

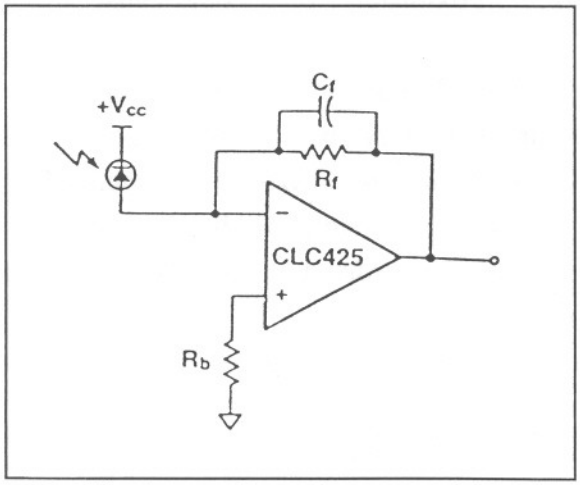


*Fig.8 Transimpedance amplifier configuration.*

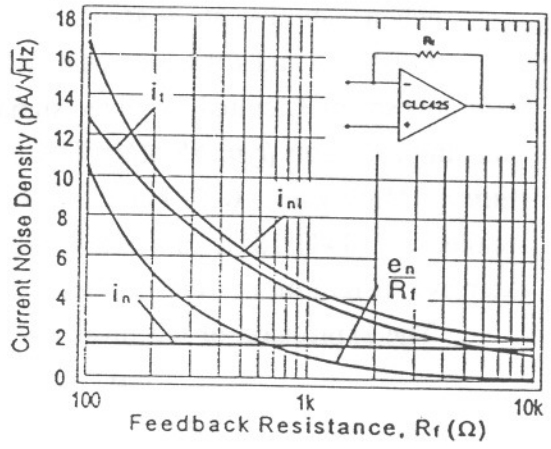


*Fig.9 Current noise density vs. feedback resistance.*

Since the amplificator is not unconditionally stable, further adjusts are necessary once loaded with the second amplification stage. However, it was possible to study the amplifier's stability through a test set-up where the amplifier worked as an inverting amplifier, rather than as a transimpedance one. So as to compensate peaking and possible oscillation, the capacitance $C_{12}$ was trimmed up to *3.5pF* [137].

| TRANSIMPEDANCE STAGE PERFORMANCE *(measured values unless otherwise indicated)* CLC425 AIB Comlinear Corp. *(voltage feedback amplifier)* | | |
|---|---|---|
| ***Gain (eq.(5)):*** | $R_f \in (750, 5750)\Omega \rightarrow (57.5, 75.2)$dB | Note: $R_f = R_{13} + R_{14}$ (Fig.2) |
| ***Bandwidth:*** | B > 10MHz | GBP = 1.9 GHz |
| ***Noise (eq.(10)):*** | $i_n$(typ) = 1.6 pA·Hz$^{-1/2}$, $e_n$(typ) < 0.95 nV·Hz$^{-1/2}$ ($I_{cc}$=17mA) | |
| | $i_{ni}$ = 5.10 pA·Hz$^{-1/2}$ at gain | $R_f$= 750 Ω |
| | $i_{ni}$ = 2.33 pA·Hz$^{-1/2}$ at gain | $R_f$= 5750 Ω |
| | *Averaged measurement* $i_{ni}$= 5.27 pA·Hz$^{-1/2}$ (independent of gain, see Sect.6.3). | |
| ***Output voltage swing:*** | ±3.8 V ($R_L \rightarrow \infty$); | ±3.0 V ($R_L \rightarrow 50\Omega$) |

***Tab.3 Transimpedance stage designed.***

## 4. CONDITIONING STAGE

Fig.2 shows the conditioning stage of the analog lidar receiver. As discussed in Chap.3, Sect.2.5.1, this second amplification stage must guarantee three important points:

**a)** Provide extra amplification (with variable gain) to the signal leaving the transimpedance stage to meet the *±1-V input dynamic range of digitizer.*

**b)** Disable the receiver until the lidar-return has not reached the minimum exploring range wished, $R_{min.}$

**c)** Filter-out frequencies over *10 MHz* approximately, that would cause aliasing when sampling at *20 Msps.*

Goals *(a)* and *(b)* have been achieved using *CLC430* op amp of Comlinear Corp. Since it is specially suited for video signal multiplexing, it has both the advantage of wide-band amplification ***(typ. 55 MHz, 2000 V/μs)*** and ***fast digital control of its enable/disable feature.*** High-gain, wide-band operation employs a current feedback (CF) based architecture [141][162], rather that the classic voltage feedback. Appendix 1, provides extensive insight on *current feedback amplifiers (CFAs).*

The expression of the inverting gain at low frequencies is given by

$$G_A = -\frac{R_f}{R_g} \; ; \qquad R_f = R_{23} \; , \quad R_g = R_{21} + R_{22} \tag{11}$$

Note that the notation used for the feedback resistor, $R_f$, is the same as in Sect.3 but they refer to different amplification stages. Tab.4 reproduces manufacturer's design point information for *CLC430*. The table lists optimum feedback transimpedance [155][156], $Z_t$, for maximum bandwidth, optimum open-loop phase margin and close-loop response flatness. With such $Z_t$, bandwidths may well be about the specified 55 MHz for a gain $A_v=2$. As for the conditioning stage, gain is wished to be as high as possible (minimum specs for the lidar receiver are given in Tab.1) provided *10-MHz* bandwidth at maximum gain (worst bandwidth) is kept. Note that the higher the gain, the better the chance to explore from larger $R_{min}$. In order to meet this end, the CFA model of Ap.1 was simulated in MATLAB using digitalized open-loop graphs from the manufacturer.

The procedure followed was the following: Starting at Tab.4, $R_g$ was lowered to *77* Ω since lower values could overload the transimpedance stage. In theory, changing the gain resistor should not degrade bandwidth but in practice, bandwidth reduction and peaking occurs. The second step, was to increase the feedback resistor $R_f$. This operation means a large reduction in bandwidth because the gain-bandwidth tradeoff for conventional voltage feedback op amps is translated for *CFAs* into a feedback resistor-bandwidth trade-off [137]. Finally, the simulations yield a gain of *26 V/V* with $R_f = 2k\Omega$ and about *20-MHz* bandwidth. In Tab.5, $Z_t$ figures for maximum and minimum gain are also shown.

| Part # | $A_v$ | $R_f(\Omega)$ | $R_i(\Omega)$ | $Z_t(\Omega)$ |
|---|---|---|---|---|
| CLC430 | +2 | 750 | 60 | 870 |
| CLC411 | +2 | 301 | 50 | 400 |

***Tab.4 Design point information.***

To corroborate the design, the graphic procedure described in Ap.1 was also used. If feedback transimpedance lines are plot over the open-loop gain plots of the amplifier (Fig.12), cross-over points result at *7-* and *10-MHz* bandwidth, which correspond to maximum and minimum gain situations, respectively. To solve this controversy, measurement of the amplification stage using the test set-up of Fig.10 revealed a *3dB* cutt-off frequency of *17 MHz* for the minimum gain *($G_A'$ = 5.3 dB)* and *13.2 MHz* for the maximum gain *($G_A'$ = 28.3 dB)*. The prime indicates that the filter gain *($G_F$= 0.673 V/V)* is not included into the conditioning gain. Thus, the net gain for the conditioning stage will be

$$G_A = G_A' G_F \tag{12}$$

Fig.11 shows frequency response of the amplifier at maximum gain. The conditioning stage has finally been implemented with these values.

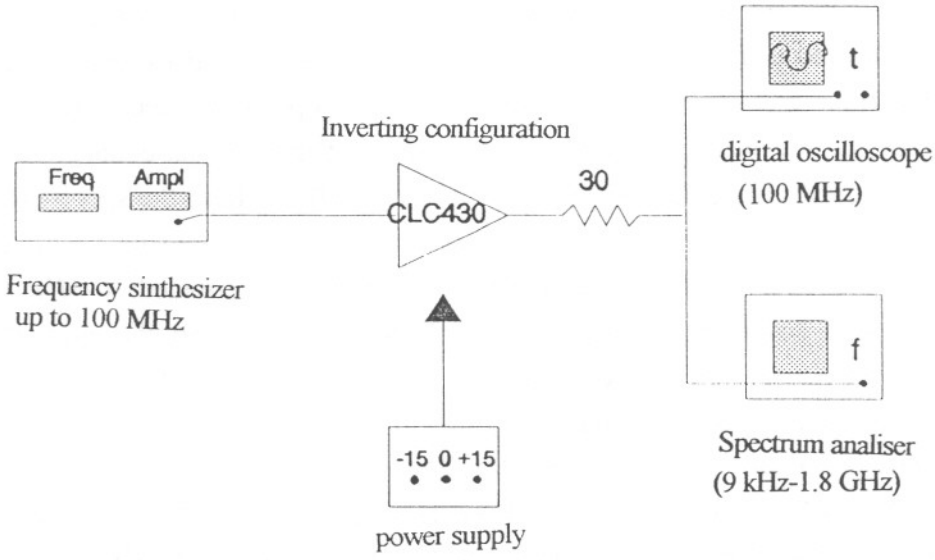


*Fig.10 Conditioning amplifier test set-up.*

Harmonic distortion measurements are also included in Tab.5.

As far as noise is concerned, the *equivalent input noise voltage density*, $e_{ni}$, may easily be computed using some results from Sect.3 and ref.[157]. Results similar to eq.(8) are obtained for the inverting configuration if $R_{s,eq}$ is replaced by $R_b$ and $R_g$ is replaced by $R_{g,eq}=R_g+R_s$ in Fig.7. With these substitutions, eq.(8) will yield an $e_{ni}$ referred to the non-inverting input. Referring $e_{ni}$ to the inverting input is easily accomplished by multiplying $e_{ni}$ by the ratio of non-inverting to inverting gains. Doing so yields,

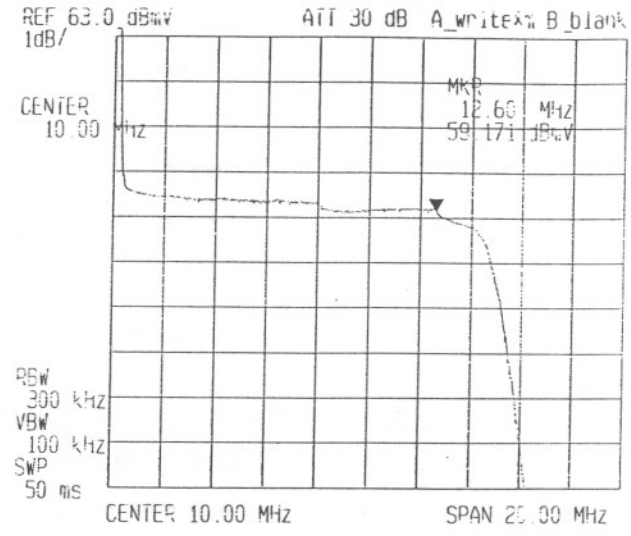


*Fig.11 Conditioning stage frequency response.*

$$e_{ni}=\sqrt{e_n^2+(i_{n+}R_b)^2+4KTR_b+(i_{n-}(R_f \parallel R_{g,eq}))^2+4KT(R_f \parallel R_{g,eq})}\left(1+\frac{R_g}{R_f}\right) \qquad (13)$$

Noise computations are shown in Tab.5 considering that $R_b$, $R_s \approx 0$ (since they are the output resistances of the *offset correction unit* and *CLC425* op amp, respectively), ($R_s$(typ) = 0.5Ω), $R_f=R_{23}$ and $R_g=R_{21}+R_{22}$ from Fig.2. Fig.13 depicts the equivalent input noise sources versus frequency including *1/f* Flicker noise.

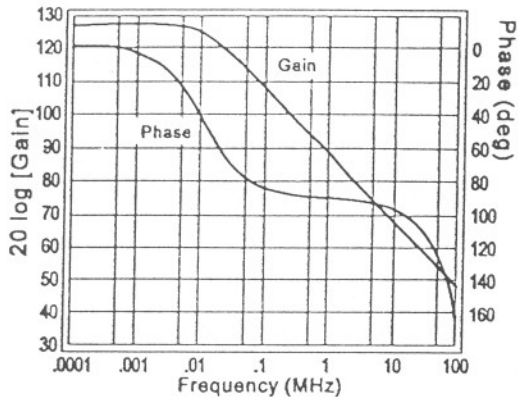


*Fig.12 Open-loop transimpedance gain.*

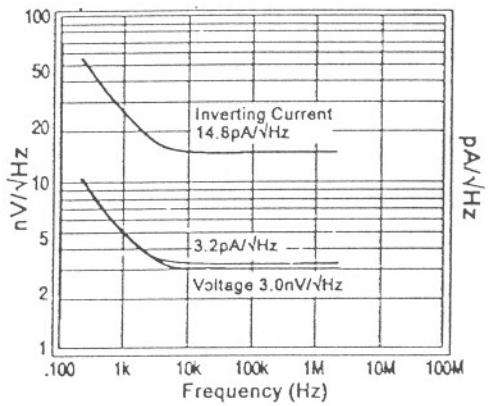


*Fig.13 Equivalent input noise.*

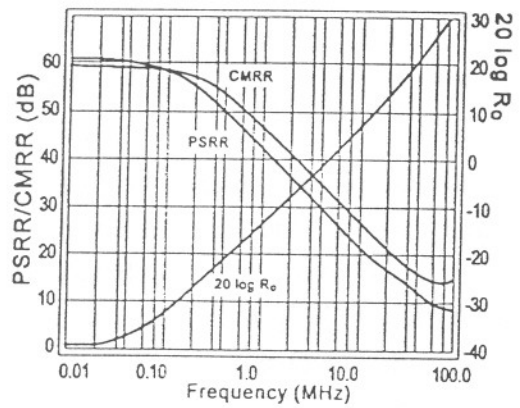


*Fig.14 CMRR, PSRR and closed loop $R_o$.*

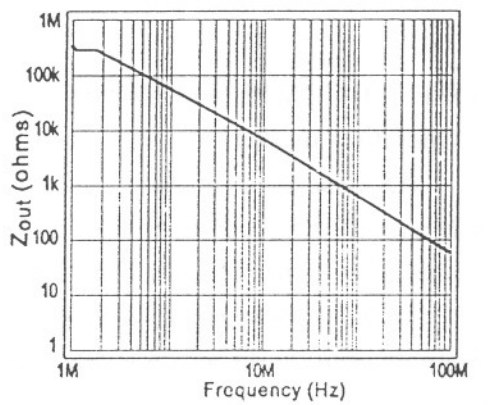


*Fig.15 Output impedance, disable mode.*

*NOTE: Illustrations show CLC430 typical performance from manufacturer's data sheets.*

**CONDITIONING STAGE PERFORMANCE**

***(measured values unless otherwise indicated)***

CLC430 AIB Comlinear Corp. *(current feedback amplifier)*

| | | | |
|---|---|---|---|
| ***Gain (eq.(11),(12)):*** | $R_{21}$ = 77Ω, $R_{22}$ = 1kΩ (variable), $R_g$=$R_{21}$+$R_{22}$, $R_f$=$R_{23}$ = 2kΩ (Fig.2) | | |
| | Inverting Gain: | $G_A'$ = (1.88, 25.97) V/V → (5.3, 28.3) dB | |
| | Filter Gain: | $G_F$ = 0.673 V/V | (not included) |
| ***Bandwidth:*** | 9.2 MHz (SCLF-8 filter); | | 13.2 MHz (without filter) |
| ***Design point (Ap.1):*** | $R_i$ = 60 Ω, $Z_t$ = 3.62 kΩΩ-2.17 kΩ (max-min gain) | | |
| ***Harmonic distortion (THD):*** | > 40 dBc (50 mVef input, 10 MHz, 2nd harmonic) | | |
| ***Noise specs (eq.(13)):*** | $i_{n+}$ = 4pA·Hz$^{-1/2}$, | $i_{n-}$ = 15pA·Hz$^{-1/2}$, | $e_n$ = 3nV·Hz$^{-1/2}$ |
| | $e_{ni}$(typ) = 17.6 nV·Hz$^{-1/2}$ | at gain | $G_A$ = -1.88 V/V |
| | $e_{ni}$(typ) = 3.5 nV·Hz$^{-1/2}$ | at gain | $G_A$ = -25.97 V/V |
| ***Output voltage swing:*** | ±13 V ($R_L$→∞); | ±11 V ($R_L$→100Ω) | |
| ***Enable/disable performance:*** (time and logic level specs from Fig.15 and $V_{cc}$ = ±15V) | | | |
| | Enable time: 200 ns (>12.7 V) | Disable time: 100 ns (<10.0 V) | |

*Tab.5 Conditioning stage designed.*

Fig.14 shows CMRR, PSRR and closed-loop output resistance. Comparing PSRR in this figure to that in Fig.5, *CLC430 has 40 dBs less isolation from the voltage supply as its CLC425 counterpart.* So, the conditioning stage is the weakest stage in front of voltage supply ripple and spikes.

As to the disable feature, Fig.15 depicts *CLC430* output impedance when disabled. Equivalently, the figure is a specification of the expected op amp isolation versus frequency when disabled. Pin 8 enable/disable logic levels are indicated in Tab.5. The amplifier is enabled with pin 8 left open due to an internal *2-k*Ω pull-up resistor.

Finally, the conditioning stage includes the SMD filter *SCLF-8* to filter out alias frequencies. Filter ripple is about *1 dB* from DC to *8 MHz*, and *3-dB* cutt-off frequency is *9.2 MHz*. During test and measurement of the receiver, resistance $R_{24}$ in Fig.2 was finely trimmed to *24.3* Ω to match the filter input impedance *(50* Ω*)* to the *CLC430* closed-loop output impedance.

## 5. OFFSET COMPENSATION STAGE

### 5.1 Operation modes

As described in Sect.2.2, a practical limitation of current-to-voltage sensing amplifiers is offset compensation. To fulfil this purpose, the lidar receiver of Fig.2 includes a low-drift precision offset compensation stage. Two operating modes are possible:

***In the normal mode,*** the inverting input of the *OP-27* (pin 2) is derived to ground and the op amp works as a non-inverting amplifier with a level shifter feature that is taken from a thermally compensated precision voltage reference. This mode of operation is illustrated in Fig.2 and will be discussed in Sect.5.2 along with system offsets. In spite of the fact that transimpedance and conditioning stage offsets can be cancelled by trimming multiturn potentiometers in the reference unit, ***thermal drift must be periodically reset.***

***The second operation mode does compensate offset thermal drifts but it is not suitable for lidar operation.*** Its application is found when the receiver works as a general purpose optical communications receiver. To set this mode the inverting input of the *OP-27* (pin 2) must be connected to the output of the lidar receiver. In addition, the lidar receiver must work on a *50-*Ω *system.* The principle of operation is very simple: the op amp compares the *dc-level* at the receiver's output to that of the reference voltage and adds an error voltage to the conditioning stage that balances the difference. Accuracy only depends on *OP-27* and *reference* drifts, which are about *20 ppm/°C* altogether. Notwithstanding the high performance, this mode of operation is only valid when the receiver is used in communications applications where dc-level is not important, such as optical links involving modulated signals. Since the correction unit virtually ties the dc-level at the receiver's output to the reference voltage, strictly speaking, the system is *band-pass.* Sect.5.2 concentrates on the auto-zero mode and on reference unit design.

### 5.2 Offset level and drift rate assessment in normal mode

A straightforward way of assessing the effect of nonzero input currents and input offset voltage upon circuit performance is to determine the *output with zero input signal* [135]. Since grounding the input makes the inverting, non-inverting and transimpedance amplifiers indistinguishable, an approach is to compute offset at the non-inverting input and then, retrace the steps back to the transimpedance and inverting configurations.

According to [135] and the notation introduced in Fig.7, the offset at the output of the non-inverting op amp can be expressed as

$$V_o = \left(1 + \frac{R_f}{R_g}\right)\left[(R_f \parallel R_g) I_n - R_s I_p + V_{OS}\right] \tag{14}$$

where:

$I_n$ is the input bias current at the negative input,
$I_p$ is the input bias current at the non-inverting input and,
$V_{OS}$ is the input offset voltage.

*Input bias current,* $I_B$, and *input offset current,* $I_{OS}$ (Sect.2.2) are defined as

$$I_B \triangleq \frac{I_p + I_n}{2} , \qquad I_{OS} \triangleq I_p - I_n \tag{15}$$

Tab.6 lists $V_{OS}$, $I_B$ and $I_{OS}$ for the op amps used in the receiver. The approximation $I_B = I_p = I_n$ is assumed.

From [135], total offset at the receiver output can be computed, which yields

$$V_o = \left[R_{f,2} I_{n,2} - R_{s,2} I_{p,2} + \left(1 + \frac{R_{f,2}}{R_{g,2}}\right) V_{OS,2}\right] - (R_{f,1} I_{n,1} + V_{OS,1}) \frac{R_{f,2}}{R_{g,2}} \tag{16}$$

where the subscripts *1* and *2* mean, transimpedance and conditioning stage, respectively.

| op amp | OFFSET VOLTAGE | | BIAS CURRENT | | OFFSET CURRENT | |
|---|---|---|---|---|---|---|
| | $V_{OS}$ | drift | $I_B$ | drift | $I_{OS}$ | drift |
| **CLC425** | +0.1(1) mV | +2(4)μV/°C | +12(20) μA | 100(120)nA/°C | ±0.2(2)μA | ±3(25)nA/°C |
| **CLC430** | +2 mV | +25μV/°C | +3 μA | ±10nA/°C | --- | --- |
| **OP-27** | ±10 μV | ±0.4μV/°C | ±10 nA | see specs | ±7nA | see specs |

***Tab.6 Typ. (max) input offsets and drifts.***

If the resistive values given in Tab.3, Tab.5 and input offsets of Tab.6 are substituted back into eq.(16), ***the transimpedance stage turns out to be responsible for the receiver offset, no matter the gain set.*** This is so, because offset from this stage suffers further amplification at the conditioning stage. In the computations, *OP-27* and photodiode dark current contibutions to offset are negligible (see Tab.6 and Tab.2).

Finally, ***receiver output offset can be approximated by***

$$V_o \approx -(G_T I_{B,T} + V_{OS,T})|G_A| \tag{17}$$

where $G_T$ and $G_A$ represent the transimpedance and conditioning gains and the subscript $T$ indicates transimpedance.

***As for the thermal drift, it can be shown that it is dominated by the input current bias of the transimpedance stage.*** Mathematically,

$$\frac{\partial V_o}{\partial T} = -|G_T G_A| \frac{\partial I_B}{\partial T} \tag{18}$$

Typical and maximum offsets and drift rates are given in Tab.7, where maximum gains in both amplification stages are assumed (worst-case estimation).

| offset (typ) | drift (typ) | offset (max) | drift (max) |
|---|---|---|---|
| -1.8 V | +15 mV/°C | -3.0 V | +18 mV/°C |

***Tab.7 Receiver offset and drift.***

Even after some warm-up time is allowed to settle the offset level at the receiver output and it is compensated for, *the thermal drift can be very important.* Thus, the typical drift of *15 mV/°C* represents *30 LSB/°C* drift in the *±1-V CompuScope digitizer.* ***Despite such a large drift, there is a way out if in addition to acquiring the whole lidar data segment, an small segment belonging to a very large range is also acquired. Since at such ranges, only steady state photometric background and receiver offsets are present, a net offset figure can be perfectly known in the control unit and compensated for (see Chap.6).***

### 5.3 Reference for the auto-zero unit

Maximum allowable reference drift for *1/2-LSB* error in the CompuScope 1012 (12-bits A/D converter) for a temperature change of *25°C* results *5 ppm/°C.* Assuming that the converter has *10 effective bits* due to signal-to-noise ratio limitations, this limit can be raised up to *20 ppm/°C* (see [120] for further insight).

With a moderate temperature performance of *20 ppm/°C* two different approaches were considered when designing the reference. In the first one, the temperature error was split equally between the zener and the amplifier. Basically, ***zener drift and op amp drift add directly to the drift error, while resistor error is only a function of how well the scaling resistors track (e.g. in a voltage divider).*** As a result, the design required moderate low drift zener and op amp with *10-ppm* resistors. Yet, this approach did not seem very encouraging, mainly because available metal film resistors track between *50-100 ppm.* The range of temperature coefficient errors for different components used to make a *10-V* reference from a *6.9-V* zener are shown in Tab.8. From the same table, one can see that metal film *1-%* resistors would bring the thermal drift above the *20-ppm/°C* spec. [111].

The second approach, which was the one followed, uses a very low drift zener, such as *LM399,* and allows the buffer amplifier and scaling resistors to cause most of the drift error. *LM399* is a moderate cost temperature stabilized IC zener with only *2 ppm/°C* drift that outputs *-6.95 V.* From Tab.6, *OP-27* op amp drift is as low as *0.4 μV/°C (typ), 1.8 μV/°C (max).* Using these devices, resistor tracking requirement can be relaxed to about *50 ppm,* allowing ordinary *1%* resistors and CERMET potentiometers to be used.

| DEVICE | ERROR | 10V OUTPUT DRIFT |
|---|---|---|
| **Zener** | **Zener Drift** | |
| LM199A | 0.5 ppm/°C | 0.5 ppm/°C |
| LM199, LM399A | 1 ppm/°C | 1 ppm/°C |
| LM399 | 2 ppm/°C | 2 ppm/°C |
| 1N829, LM3999 | 5 ppm/°C | 5 ppm/°C |
| LM129, 1N823A, 1N827A, LM329A | 10–50 ppm/°C | 10–50 ppm/°C |
| LM329, 1N821, 1N825 | 20–100 ppm/°C | 20–100 ppm°C |
| **Op Amp** | **Offset Voltage Drift** | |
| LM725, LH0044, LM121 | 1 μV/°C | 0.15 ppm/°C |
| LM108A, LM208A, LM308A | 5 μV/°C | 0.7 ppm/°C |
| LM741, LM101A | 15 μV/°C | 2 ppm/°C |
| LM741C, LM301A, LM308 | 30 μV/°C | 4 ppm/°C |
| **Resistors** | **Resistance Ratio Drift** | |
| 1% (RN55D) | 50–100 ppm | 20–40 ppm/°C |
| 0.1% (Wirewound) | 5–10 | 2–4 ppm |
| Tracking 1 ppm Film or Wirewound | — | 0.4 ppm/°C |

***Tab.8 Drift error contribution from reference components for a 10V reference [110].***

A four-wire *Hewlett-Packard 3478A* multimeter was used to measure the drift. Once the fine potentiometer ($R_{39}$ in Fig.2) was trimmed to adjust an output of *-1.0000 V,* no drift was observed even approaching a soldering iron. From this simple experiment, much less that *100-ppm/°C* drift can be guaranteed.

Finally, the *offset level at the receiver output in the auto-zero mode* can be assessed by grounding the input of the conditioning stage. It yields:

$$V_o = \frac{K_1(1+K_2)}{1+K_1K_2}(V_{OS27}+V_{REF}) + \frac{V_{OS}}{1+K_1K_2} \tag{19}$$

where

$$K_1 = G_F(1+G_A)\ , \qquad K_2 = G_{OP27} = \frac{R_{32}}{R_{31}} \tag{20}$$

$V_{OS}$ is the receiver offset without *auto-zero* given by eq.(17), $V_{OS27}$ is the *equivalent offset* at the *OP-27* inverting input (Tab.6) and $V_{REF}$ is the reference voltage *(-1V).* Since $G_{OP27}$ is very large (usually, the open-loop gain), eq.(19) becomes

$$V_o = V_{OS27}+V_{REF} - \frac{V_{OS430}}{K_2} \tag{21}$$

***Hence, receiver offset is basically dominated by the reference offset and drift*** ([114][110]).

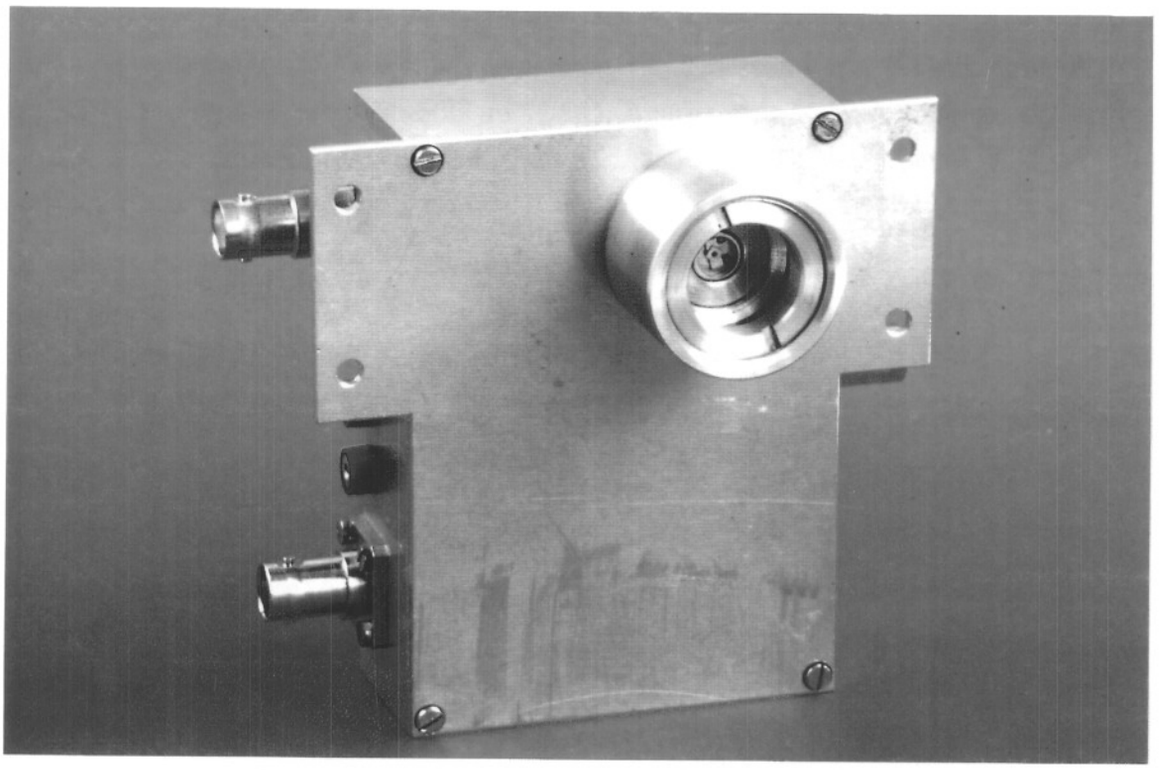

*Fig. 16 Mechanics of the lidar receiver.*

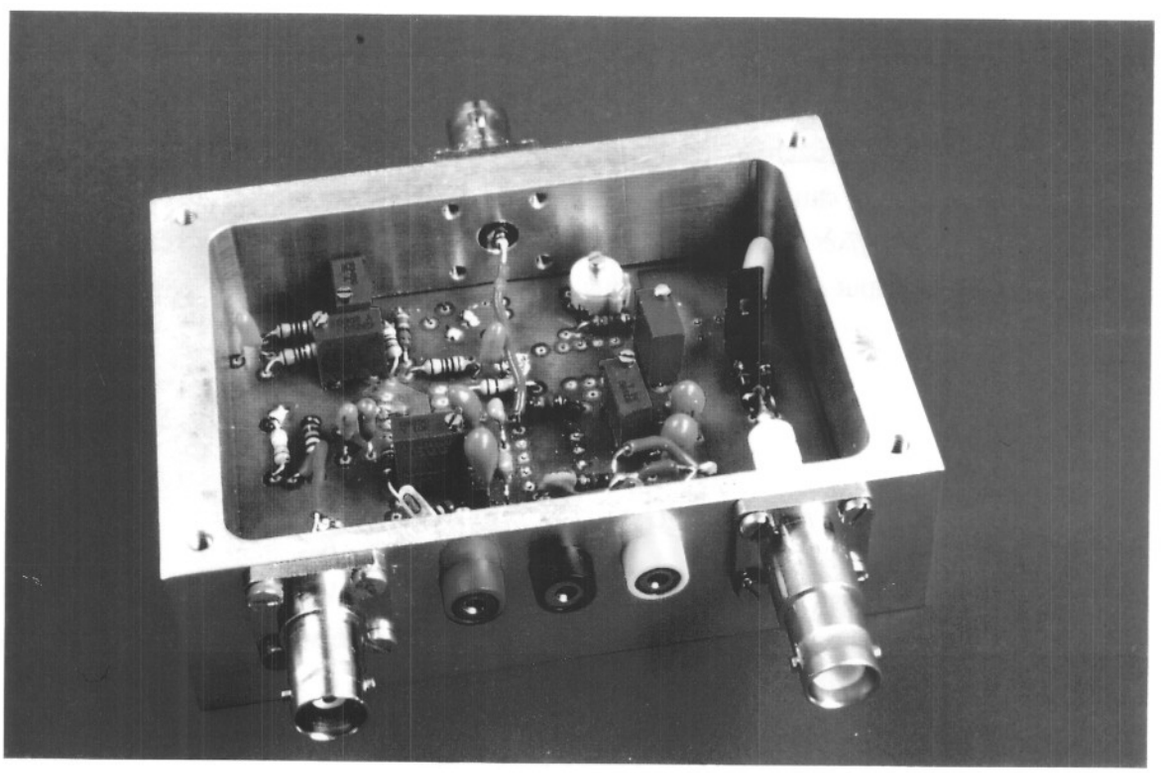

*Fig. 17 Lidar receiver circuit (top side).*

## 6. PROTOTYPE AND FINAL MEASUREMENTS

### 6.1 Mechanical overview

Prototype mechanics were of great concern during the conception of the lidar receiver. The goal was twofold: On the one side, the mechanical body should be simple and light enough to be mounted in the ocular support of the receiving telescope and on the other side, it should include facilities to be assembled in the focal plane of an ordinary reflex camera. This would greatly simplify test, measurement and alignment of the prototype using laser sources readily available in the laboratory. The prototype, which is made of aluminium, is shown in Fig.16.

To fulfil the former objective, the prototype uses a *31.6-mm* cylinder that can be screwed onto the receiver's body and assembled into the telescope's ocular. The inner side of the cylinder is also used to hold a *1-in.* diameter interference filter which is tightened by a special nut screwed on.

As for the second objective, the top side of the receiver has two swings that help attachment to the rear part of the camera. The photodiode is mounted on a special basis that enhances heat exchange. The photodetector plane is about *2 mm* higher than the real height of the focal plane of the camera. This security margin can be offset by focusing the objective of the camera, so that any bundle of parallel rays entering the objective can accurately be focused onto the photodetector. In Fig.19 the receiver is shown assembled to the camera during a measurement test.

The receiver circuit is shown in Fig.17. The connectors are: BNC signal output, BNC synchro, SHV high voltage supply input and $\pm 15$-*V* supply.

### 6.2 Bandwidth measurement

Measurement of the lidar receiver frequency response, *H(f),* is based on the test sep-up of Fig.18 and Fig.19.

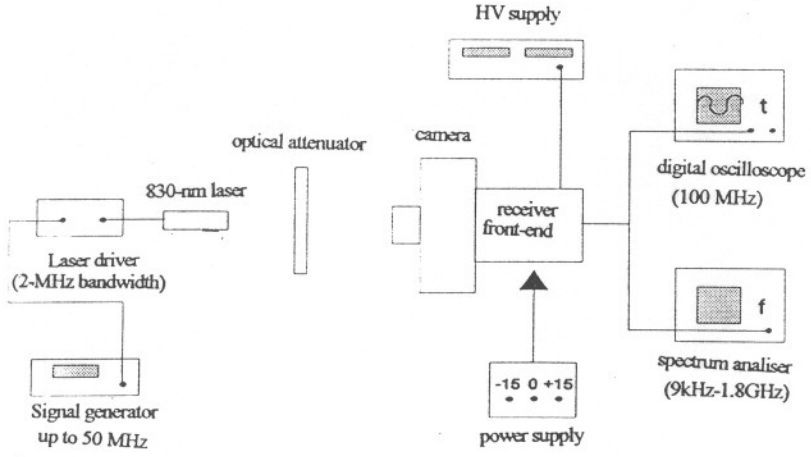


*Fig.18 Test set-up to characterize the lidar receiver.*

The test set-up includes an *830-nm IR-laser*, which is modulated by a *50-MHz* function generator using a driver [205]. Light level in the optical path is adjusted by means of the driver itself, the optical attenuator and the camera diaphragm. An infrared CCD camera is used to help alignment of the system.

All points settled, the main difficulty of the measurement was to compensate for the laser-driver low frequency response, which was much less that the receiver bandwidth. The measurement procedure followed these steps:

1) Driver frequency response characterization, $H_{driver}(f)$. A *Mod.713A-4 optoelectronic receiver* from *Analog Modules,* whose bandwidth is *200 Hz-300 MHz,* was used.

2) Measurement of the total frequency response, $H_{tot}(f)$.

$$H_{total} = H_{driver} + H(f) \qquad [dB] \tag{22}$$

3) Lidar receiver frequency response characterization, $H(f)$. From eq.(22) above, $H(f)$ can be determined by simple difference between total and laser driver frequency response. Note that photodetector bandwidth *(typ.500 MHz)* is much higher than the lidar receiver one and hence it is not taken into account.

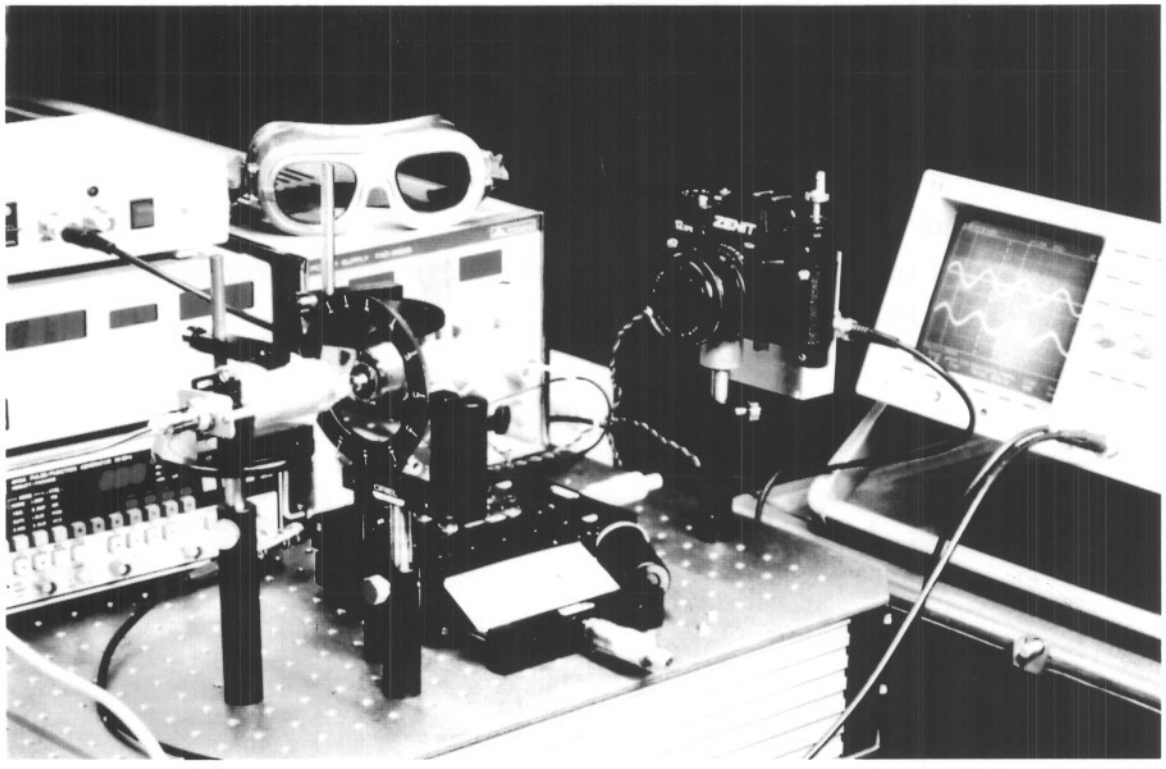

*Fig.19 Test and measurement of the lidar receiver.*

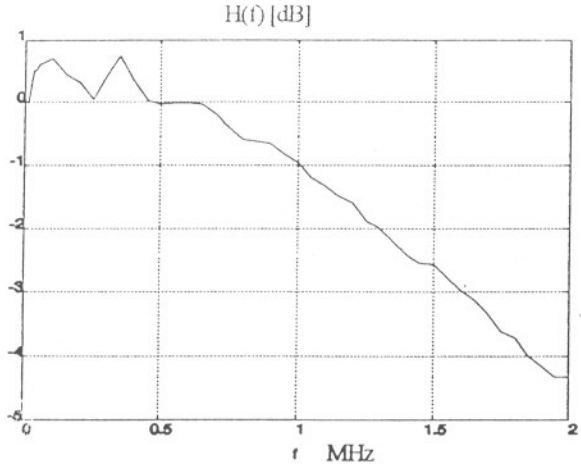


*Fig.20 Driver frequency response.*

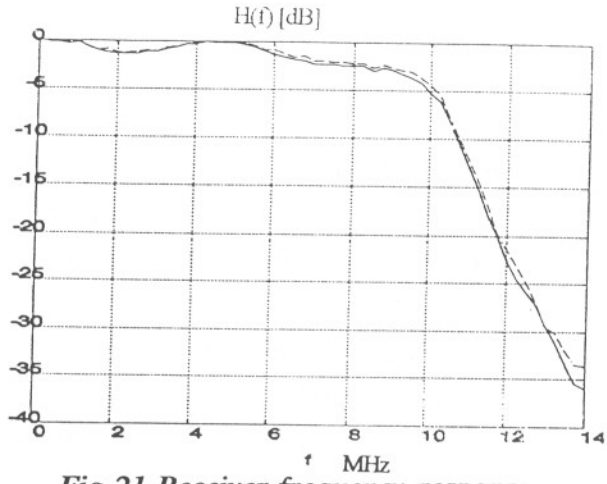


*Fig.21 Receiver frequency response.*

Fig.20 shows $H_{driver}(f)$ from *0 to 2 MHz. 3-dB* cutt-off frequency is about *1.6 MHz.* Measurement of the receiver response, *H(f)* has been done for different photodiode polarizations between *-15 V* and *-375 V.* In particular, the *APD* works as a *PIN* photodiode for a polarization of *-15 V* and as an *APD* for the manufacturer's typical polarization of *-375 V.* Fig.21 shows frequency performance of the lidar receiver, *H(f),* for *-375 V* polarization. Solid and dashed lines represent *H(f)* for two positions of the APD jumper, $R_{APD}$= *10 kΩ* and $R_{APD}$= *0 Ω,* respectively. It is evidenced that $R_{APD}$ has no effect at all on system bandwidth. Similar results were obtained for the polarization of *-15 V.*

### 6.3 Noise measurements

To measure thermal noise spectral densities at the receiver output, a *Hewlett-Packard 8590 D* spectrum analyser was used. It was set to the following values: centre frequency *5 MHz,* span *10 MHz,* resolution bandwidth, *RBW = 100 kHz* and video filter average *100 samples.* Since the video filter is a post-detection filter its setting does not change the measure of the noise level but enhances the reading [130].

The measurement was made for the four combinations of minimum and maximum gain in both transimpedance and conditioning stages. The receiver case was opened and the receiver was permanently enabled (without synchronization). Under these circumstances, it is thought that IC heating of the conditioning could be responsible for a blurred oscillation around *9-10 MHz* when maximum gains where set in both amplification stages. So as to avoid this effect, the transimpedance stage was not raised to the maximum gain of $G_T$= *5750 Ω,* but $G_T$= *4000 Ω* instead.

Tab.9 compares noise density at the receiver output to the measured values. The former can formally be computed using the expression

$$e_o = \sqrt{\left(i_{ni} G_T G_A\right)^2 + \left(e_{ni} G_A\right)^2} \qquad \left[\frac{V}{\sqrt{Hz}}\right] \tag{23}$$

where $G_T$ is the transimpedance gain, $G_A$ is the conditioning gain including filter losses (eq.(12)) and $i_{ni}$, $e_{ni}$ are the equivalent input noise densities of the transimpedance and conditioning stage, already defined. Their contributions to total noise are also indicated in Tab.9 by the products $i_{ni} \cdot G_T \cdot G_A$ and $e_{ni} \cdot G_A$, respectively. Measured figures are in close agreement with the predicted ones with the only exception of the measurement made when both stages were set at maximum gain. The risk of oscillation for such gain could explain the mismatch. Nevertheless, note that the predicted values are more pessimistic, since noise should be maximum at maximum gain.

| TRANSIMPEDANCE | | | CONDITIONING | | $e_o$ THEORY | | $e_o$ MEASUREMENT | |
|---|---|---|---|---|---|---|---|---|
| # | $G_T$ | $i_{ni} \cdot G_T \cdot G_A$ * | $G_A$ | $e_{ni} \cdot G_A$ * | budget * | eq.(23) * | $e_o$ * | dBμV |
| 1 | 750 | 4.8 | 1.88 | 22.3 | **6.6** | **22.8** | 25.7 | 18.2 |
| 2 | 750 | 63.9 | 25.97 | 61.4 | **91.2** | **90.7** | 77.6 | 27.8 |
| 3 | 4000 | 13.1 | 1.88 | 22.3 | **27.0** | **25.8** | 26.3 | 18.4 |
| 4 | 4000 | 181.1 | 25.97 | 61.4 | **373.2** | **191.2** | 55.0 ** | 24.8 |

(*) Noise densities are expressed in $nV \cdot Hz^{-1/2}$ units. (**) Low confidence measurement.

***Tab.9 Comparison among link-budget, eq.(23) and measured noise.***

The *budget column* compares link-budget values discussed in Chap.3 with their exact computation according to eq.(23) and the measurements. Note that link-budget computations rely on a simplified case where input noises of each amplification stage are independent of gain. Specially at long ranges where noise specs are more important, figures are in close agreement. Tab.3. Chap.3 densities are $i_{ni} = 5.27\,pA \cdot Hz^{-1/2}$, $e_{ni} = 3.41\,nV \cdot Hz^{-1/2}$.

For moderate gains of the receiver chain (i.e $G_T = 4000\ \Omega$ and $G_A = 8$), the product $i_{ni} \cdot G_T \cdot G_A$ would be twice $e_{ni} \cdot G_A$. ***Therefore, receiver noise is dominated by photodiode and transimpedance noise performance for moderate and high gain of the receiver*** and excellent performance at long ranges is guaranteed.